Supporting Information

Pt Single Atoms Dispersed in a Hybrid MOFox-in-Nanotube Structure for Efficient and Long-Term Stable Photocatalytic H_2 Generation

*Shanshan Qin[1#], Junli Guo[2#], Xuewen Chen[1,3], Ran Cao[4], Nikita Denisov[1], Yan-Yan Song[2], and Patrik Schmuki[1,5]**

[1]Department of Materials Science WW4-LKO, Friedrich-Alexander-University of Erlangen-Nuremberg, Martensstrasse 7, 91058 Erlangen, Germany

[2]College of Sciences, Northeastern University, Shenyang 110004, China.

[3]Department of Materials Function and Design, Nagoya Institute of Technology, Gokiso-cho, Showa-ku, Nagoya, Aichi 466-8555, Japan

[4]State Key Laboratory for Modification of Chemical Fibers and Polymer Materials, College of Materials Science and Engineering, Donghua University, Shanghai 201620, China.

[5]Regional Centre of Advanced Technologies and Materials, Šlechtitelů 27, 78371 Olomouc, Czech Republic

*Corresponding author: schmuki@ww.uni-erlangen.de

[#]*Shanshan Qin* and *Junli Guo* contributed equally to this work.

Experimental Section

Preparation of TiO_2 nanotubes (NTs): TiO_2 NTs were grown from Ti foils (15 mm × 15 mm × 0.1 mm, 99.99% trace metals basis) by electrochemical anodization. For this purpose, the Ti foils were first sequentially rinsed with acetone, ethanol, and deionized water, and then dried in air. Anodization was carried out in ethylene glycol/lactic acid /water electrolyte (H_2O content of 2.7 vol%) containing 0.1 M NH_4F (≥99.99% trace metals basis) at 120 V for 15 min.

Synthesis of MOFox-in-tube structure: The growth of MIL-125-NH_2 was carried out through a classical solvothermal reaction. BDC-NH_2 (100 mg, 99%) and HCl (200 µL, 0.1 M) were dissolved in 10 mL of a mixture of DMF (9 mL, 99.8%) and methanol (1 mL, 99.9%) in a 50 mL Teflon-lined autoclave. Then, TiO_2 NT samples were added to the solution. The sealed vessel was kept at 150 °C for 24 h to grow MOFs in TiO_2 NTs. After cooling down to room temperature, the resulting hybrid was washed with DMF and methanol for three times each, followed by drying in vacuum at 80 ^oC overnight to obtain samples of MOF-in-tube structure. Finally, the sample was annealed at different temperatures between 400 ^oC and 800 ^oC for 2 h in air to obtain MOFox-in-tube structures.

Single atom (SA) deposition on MOFox-in-tube structure (Pt@MOFox-in-tube): For the Pt SA deposition, either 0.005 mM or 2 mM solutions of $H_2PtCl_6 \cdot 6H_2O$ in deionized water were prepared. After purging the solutions with Ar gas, the obtained MOF-in-tube structures were immersed in the prepared solutions and kept for 1 h in dark in a deaerated quartz cell. Upon completion, the samples were thoroughly rinsed with deionized water and dried with nitrogen stream. In a reference experiment, the MOF-in-tube structure was first immersed in a 2 mM $H_2PtCl_6 \cdot 6H_2O$ solution and then annealed at 400 ^oC for 2 h in air.

Photocatalytic H_2 evolution by Pt@MOFox-in-tube and Pt@tube structures: In order to evaluate the photocatalytic H_2 generation performance, Pt@MOFox-in-tube structure annealed at different temperatures was irradiated with a 365 nm LED (power intensity: 65 mW cm^{-2}) and the full spectrum simulated sunlight AM 1.5 (power intensity: 100 mW cm^{-2}) in a 10 mL 50 vol% methanol solution in a sealed quartz reactor (illumination area of LED is 0.785 cm^{-2}). Evolved H_2 was determined by a gas chromatograph (GCMS-QO2010SE, SHIMADZU) with a thermal conductivity detector (TCD).

Characterization: High-angle annular dark-field scanning transmission electron microscopy (HAADF-STEM) images were acquired using an aberration-corrected Thermo Fisher Scientific Spectra 200 transmission electron microscope operated at 200 keV. The distribution of Pt SAs on the surface of the samples was further studied by scanning transmission electron microscopy energy-dispersive X-ray spectroscopy (STEM-EDX). The morphology and the chemical composition of the samples were investigated by field-emission scanning electron microscope (FESEM, S-4800, Hitachi, Japan) equipped with an energy dispersive X-ray detector (EDX Genesis, fitted to SEM chamber). Crystallinity of the samples was characterized by X-ray diffraction (XRD, X'pert Philips PMD diffractometer) operating with graphite monochromatized Cu irradiation (wavelength: 0.154056 nm). Chemical composition of the samples and oxidation states of the SAs were studied by X-ray photoelectron spectroscopy (XPS, PHI 5600), and the recorded XPS spectra were shifted to a standard Ti 2p peak position of 458.5 eV in anatase. XPS peak fitting was carried out using MultiPak software. Absorbance spectra of photocatalysts were measured by a fiber-based UV–vis-IR spectrophotometer (Avantes, ULS2048) equipped with an integrating sphere AvaSphere-30 using AvaLight-DH-S-BAL balanced power light source. For solid current-voltage (I-V) measurements, MOFox powder electrode was fabricated using 0.2 mg photocatalysts of

MOFox powder in a water/ethanol =50:50 Nafion slurry that placed on a carbon electrode. Solid-state conductivity measurements were carried out by a 2-point measurement setup which consisted of a USMCO micromanipulator and precision semiconductor parameter analyzer (4156C, Agilent technologies, Japan). All I-V curves were measured with 20 mV/s sweep rate in the voltage window from -2 V to 2 V.

Synthesis of MOF (MIL-125-NH_2) powder: 1.5 mM titanium (IV) isopropoxide (Acros Organics, 98%) and 3 mM 2-aminoterephthalic acid $HO_2CC_6H_3NH_2$-CO_2H (Aldrich, 99%) were added to the mixture of methanol (Aldrich, 99.9%) and DMF (99.8%, Acros Organics, extra-dry) with a volume ratio of 9:1. The slurry was then transferred to a 125 mL Teflon liner, which was further introduced into a metallic Parr bomb. The system was heated overnight (16 h) at 150 °C. The resulting light-yellow product was filtered off, washed with DMF to remove the excess of unreacted organic ligand, then washed again with methanol to exchange DMF with methanol, which is more volatile and easily removable by moderate heating.[1]

Synthesis of Pt SA decorated MOFox powder (Pt@MOFox): For producing a Pt SA loaded MOF-powder reference we followed a procedure by Liu et al.[2] – the characterization of the MOF powder is given in Figure S2. The inset of Figure 2c shows a SEM of the obtained MOFox powder with a typical crystallite size of approximately 150 nm. Typically, 60 mg of MIL-125-NH_2 particles were dispersed in a 2 mM $H_2PtCl_6 \cdot 6H_2O$ aqueous solution (20 mL) and stirred for 3 h for encapsulated precursor synthesis. The resulting materials were then centrifuged, washed with deionized water, and dried at 70 ^oC. Finally, the Pt SA-decorated TiO_2 particles were obtained by annealing at 400 ^oC for 4 h in air.[2]

Synthesis of anatase TiO_2 nanotubes decorated with Pt single atoms (Pt@tube): TiO_2 NTs were grown that were first annealed at 400 °C and then exposed to the hydrothermal

treatment in 150 °C for 24 h (referred as Pt@tube). Using this experimental sequence, no MOF growth takes place inside the NTs (see Figure S9) as in-situ MOF formation relies on the partial solubility of amorphous TiO_2 NT walls.

Photocatalytic H_2 evolution by Pt@MOF and Pt@MOFox powders: In order to evaluate the photocatalytic H_2 generation performance of powder samples, 2 mg photocatalysts of Pt@MIL-125-NH_2 or Pt@MOFox TiO_2 powders were ultrasonically dispersed in a 10 mL methanol/water mixture (volume ratio 1:1) in a sealed quartz reactor and irradiated with a 365 nm LED (illumination area of LED is 0.785 cm^{-2}, power intensity is 65 mW cm^{-2}). The slurry kept continuously stirring during illumination for H_2 evolution. Evolved H_2 was determined at specific time intervals by a gas chromatograph (GCMS-QO2010SE, SHIMADZU) with a thermal conductivity detector (TCD).

Dye desorption measurements: The annealed samples were immersed into an acetonitrile/tert-butanol mixture (volume ratio 1:1) containing 0.3 mM Ru-based dye (cis-bis(isothiocyanato) bis(2,2-bipyridyl 4,4-dicarboxylato) ruthenium(II) bistetrabutylammonium (D-719, Eversolar, Taiwan) for 24 h at 40°C. The dye-sensitized samples were rinsed with acetonitrile to remove the non-chemisorbed dye molecules and gently dried with nitrogen stream. Then the dye desorption was carried out by immersing the dye-sensitized samples into a 10 mM KOH solution (5 ml) for 24 h. The absorption spectrum of the dye released into the KOH solution was then measured by Perkin Elmer Lambda XLS+ UV-vis spectrometer (using the spectrum of a 10 mM KOH solution as a background). Dye loading amount was further calculated by the following equation:

$$C = \frac{A}{\varepsilon * l} \tag{1}$$

$$M = C \times V \tag{2}$$

where A is the measured absorption of the dye solution, ε is the molar attenuation coefficient (ε = 14100 L mol^{-1} cm^{-1} at λ = 515 nm), l is the light path length in the solution (l = 1 cm), C is the concentration of the dye solution, and M is the dye loading.

Photoelectrochemical studies: MOFox powder or MIL-125-NH_2 electrodes for the photoelectrochemical characterization were fabricated using 0.2 mg photocatalysts of MOFox powder in a water/ethanol =50:50 Nafion slurry that placed on a carbon electrode. MOFox-in-tube structure and Pt@tube can be used directly as an electrode. The electrode then was placed in a 3-electrode photoelectrochemical cell as a working electrode. An Ag/AgCl electrode was used as a reference electrode and a Pt plate as a counter electrode. 0.1 M Na_2SO_4 dissolved in distilled water was used as electrolyte and the applied potential was 0.5 V vs. Ag/AgCl. Illumination was provided by a 150 W Xe arc lamp (LOT-Oriel Instruments) with a Cornerstone motorized 1/8m monochromator. The monochromatized light was focused on a 5×5 mm^2 spot onto the sample surface through a quartz light-pass window in the electrochemical cell. At each wavelength, a photocurrent transient was acquired and the steady state photocurrent was recorded. Photocurrent transients were recorded for 20 s using an electronic shutter system and A/D data acquisition.

To characterize the performance of differently treated samples, incident photon-to-current conversion efficiency (IPCE) is characterized. In the case of photoelectrochemical water splitting, IPCE describes the maximum possible efficiency with which incoming radiation can produce hydrogen from water (assuming that all electrons are used for the hydrogen evolution),[3] and can be calculated as follows:

$$IPCE\ (\%) = (J_{ph} \times hv/I \times \lambda) \times 100 \quad (3)$$

where J_{ph} (mA cm^{-2}) is the photocurrent density, hv (1240 eV nm^{-1}) is the photon energy of the incident light, I (W cm^{-2}) is the irradiance of the electrode surface, and λ (nm) is the wavelength of the light.

Photocurrent decay curves were fitted with a bi-exponential function:[4]

$$J(t) = J_\infty + J_0\left[\alpha e^{-k_1(t-t_0)} + (1-\alpha)e^{-k_2(t-t_0)}\right] \quad (4)$$

where J_∞ – background current density, J_0 – onset current density, α – factor determining the relative weight of each of the two exponentials, k_1, k_2 – rate constants corresponding to decay kinetics for each of the two exponentials (larger k values correspond to faster decay), t – experiment time, t_0 – onset time of the photocurrent decay.

For intensity-modulated photocurrent spectroscopy (IMPS) measurements, illumination was performed at λ = 358 nm at stable background intensities (in the range 7.5–77.6 μW cm^{-2}) with superimposed sinusoidal oscillations (with amplitude equal to 10% of the background intensity) in the frequency range of 0.1–1000 Hz. Transport time constant (τ_c) values were determined from the IMPS plots using the formula:

$$\tau_c = (2\pi f_{min})^{-1} \quad (5)$$

where f_{min} is the intensity oscillations frequency at which the lowest imaginary photocurrent efficiency (imaginary H) was measured.

Electrochemical impedance spectroscopy (EIS) measurements were performed in dark at an average potential of -0.65 V (vs. Ag/AgCl), which corresponds to the flat-band potential of TiO_2.[5] During the measurements, periodic oscillations with an amplitude of 10 mV and frequency in the range of 10^{-2}-10^3 Hz were superimposed to the applied potential (-0.65 V), and the impedance response at each frequency was recorded. The recorded EIS Nyquist plots were further fitted with a single time constant (Randles) equivalent circuit model comprising a series resistance (R_s), charge transfer resistance (R_{ct}), and a double layer capacitance (C_{dl}), using "EIS Spectrum Analyzer" software.[6]

Calculation of MOF content: The loading amount (χ) of MOFs in the composite membrane is calculated from the following equation:

$$\chi = \frac{M_{mof}}{M_{mof} - M_{oxide}} \times W_{loss} \quad (6)$$

where M_{mof} is the molecular weight of MOF, M_{oxide} is the molecular weight of the residual oxide after thermal decomposition of MOF, W_{loss} is the weight loss obtained from the TGA curve.

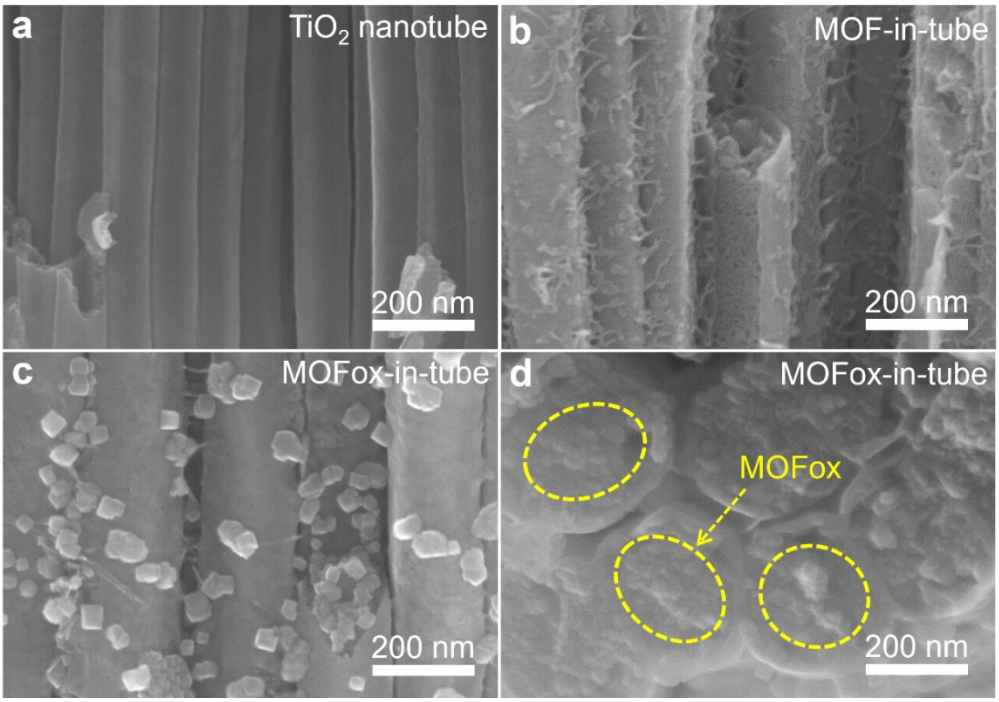

Figure S1. Cross-sectional SEM images of (a) TiO_2 nanotube, (b) MOF-in-tube, and (c) MOFox-in-tube (400 °C) samples. (d) SEM image showing the structure of MOFox formed inside the nanotubes.

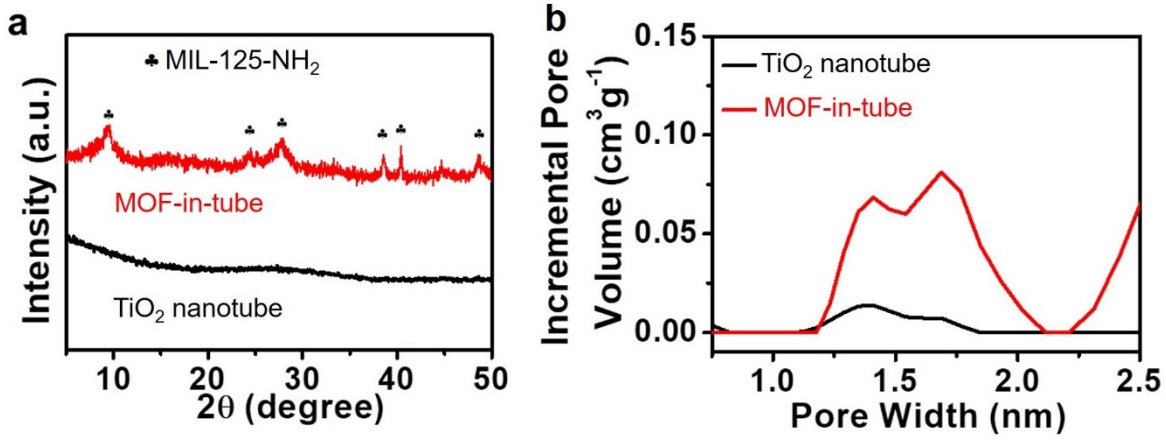

Figure S2. (a) XRD patterns and (b) pore size distribution of TiO_2 nanotube and MOF-in-tube.[7]

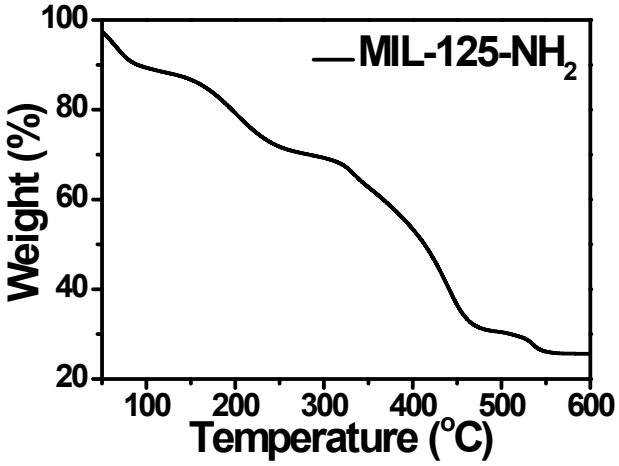

Figure S3. Thermogravimetric analysis (TGA) of MIL-125-NH_2 powder.[8]

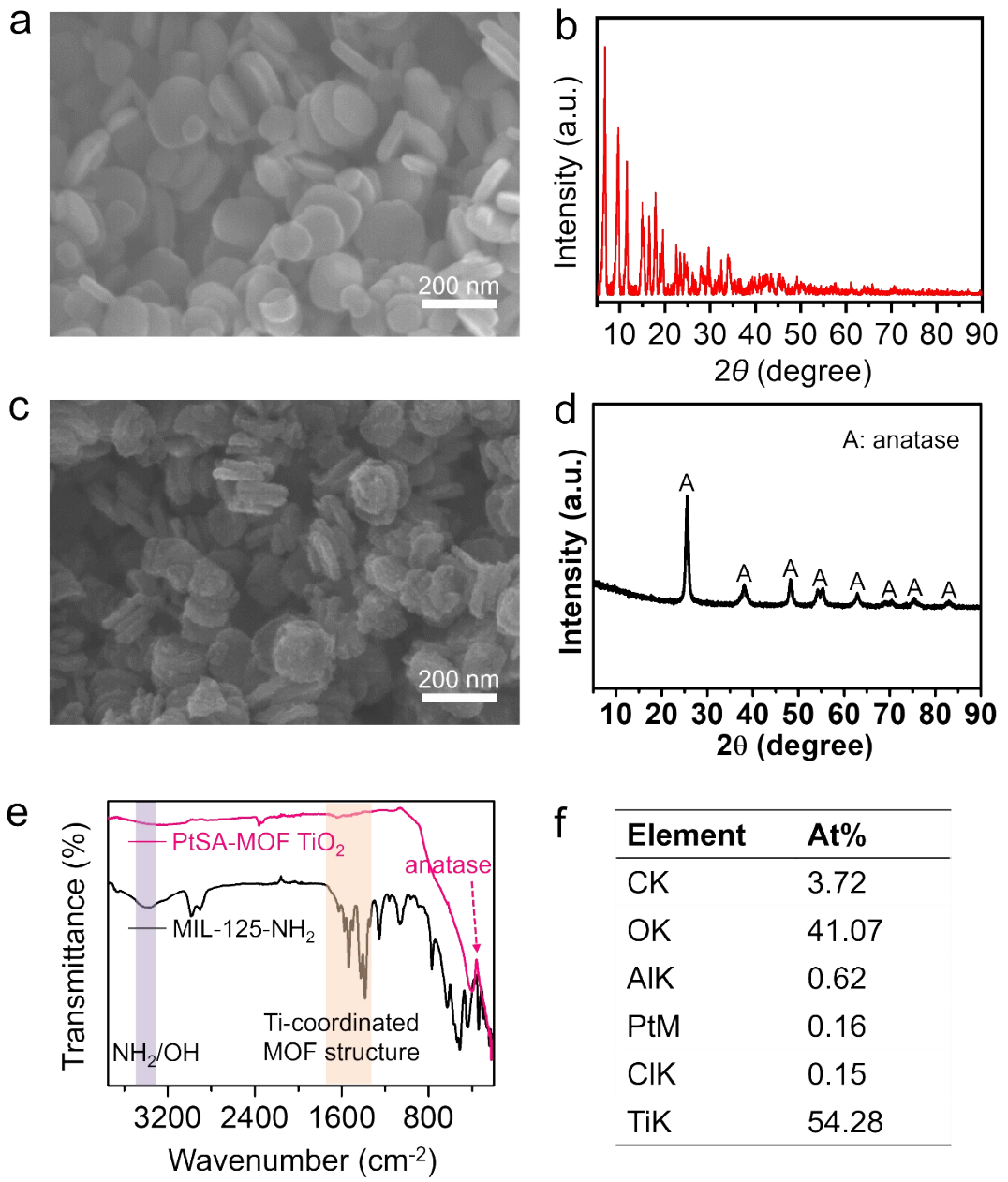

Element	At%
CK	3.72
OK	41.07
AlK	0.62
PtM	0.16
ClK	0.15
TiK	54.28

Figure S4. (a,c) SEM images and (b,d) XRD patterns of MIL-125-NH_2 powder and Pt@MOFox (MIL-125-NH_2 powder annealed at 400 °C in air for 4 h, followed by Pt SA deposition using 2 mM H_2PtCl_6 solution), respectively. (e) FTIR spectra of MIL-125-NH_2 powder and Pt@MOFox TiO_2. (f) Elemental composition of Pt@MOFox measured by EDX.

Although MIL-125-NH_2 as an excellent photocatalyst has been reported by Mellot-Draznieks et al.,[9] most of NH_2-MOFs show very bad electronic properties (e.g. poor electrical conductivity of the coordinated organic linkers).

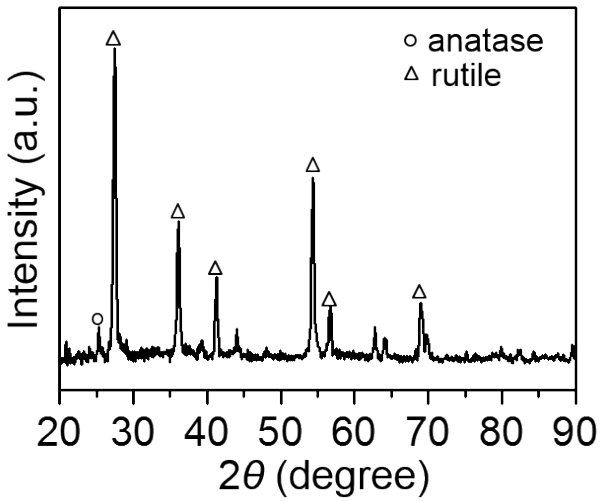

Figure S5. XRD pattern for MIL-125-NH_2 annealed at 700 °C for 4 h in air.

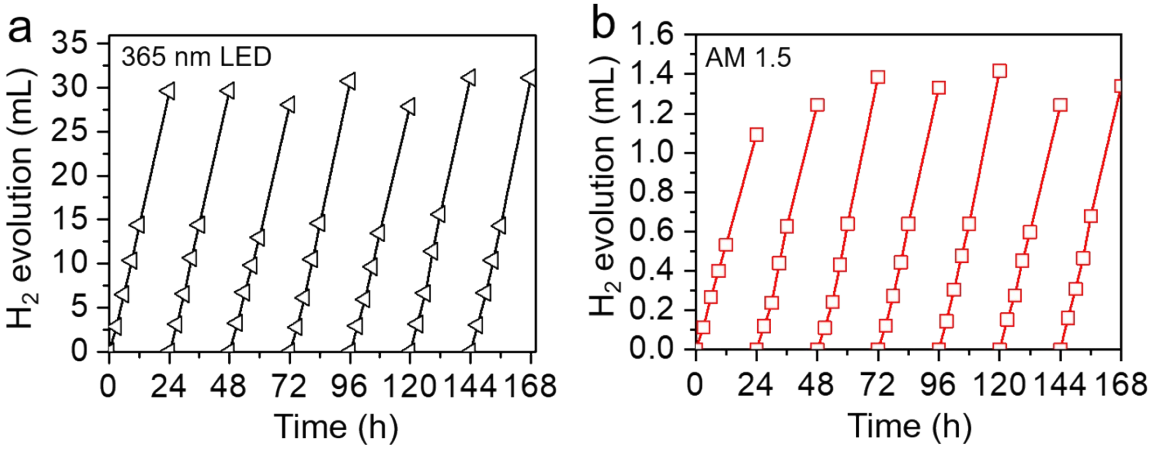

Figure S6. Long-term photocatalytic H_2 evolution performance of Pt@MOFox-in-tube structures (annealed at 400 °C) under illumination of (a) 365 nm LED (65 mW cm^{-2}) and (b) sunlight simulated AM 1.5 (100 mW cm^{-2}).

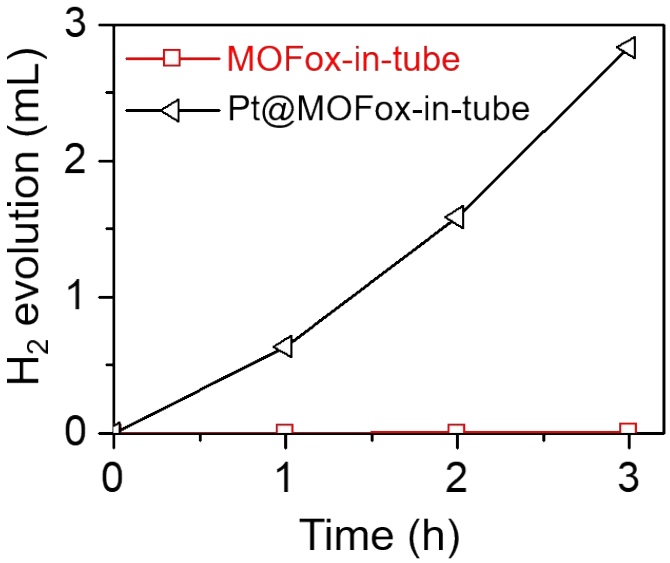

Figure S7. Comparison of photocatalytic H_2 evolution of MOFox-in-nanotubes with and without Pt decoration (Pt deposited in 2 mM H_2PtCl_6 solution).

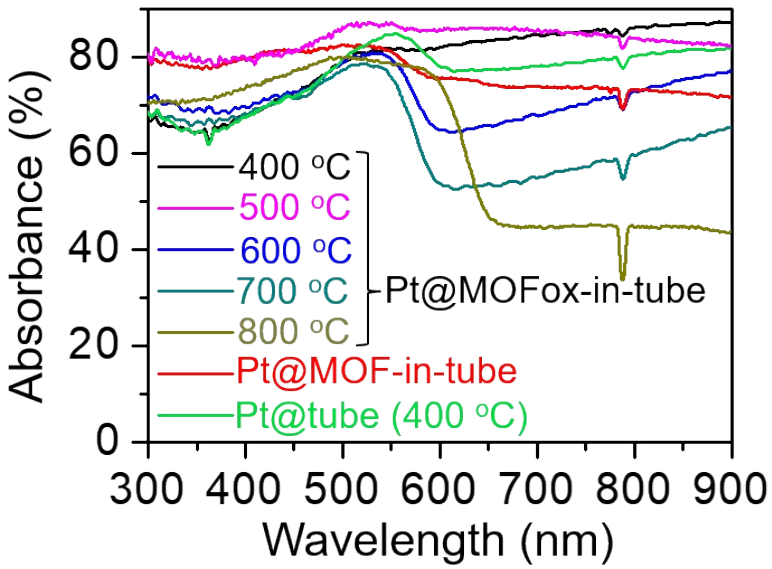

Figure S8. Absorption spectra for Pt@MOFox-in-tube and Pt@tube samples annealed at different temperatures.

The absorbance at 365 nm varies in the range of 60-80% - this is a reasonably narrow range (considering the inherent errors associated with absorbance measurements in reflection mode, and additional light scattering effects by the supporting Ti metal foil). The lack of correlation between light absorption and the H_2 evolution activity therefore indicates, that a combination of factors is in play, such as carrier transport, surface area, Pt SA dispersion and stability.

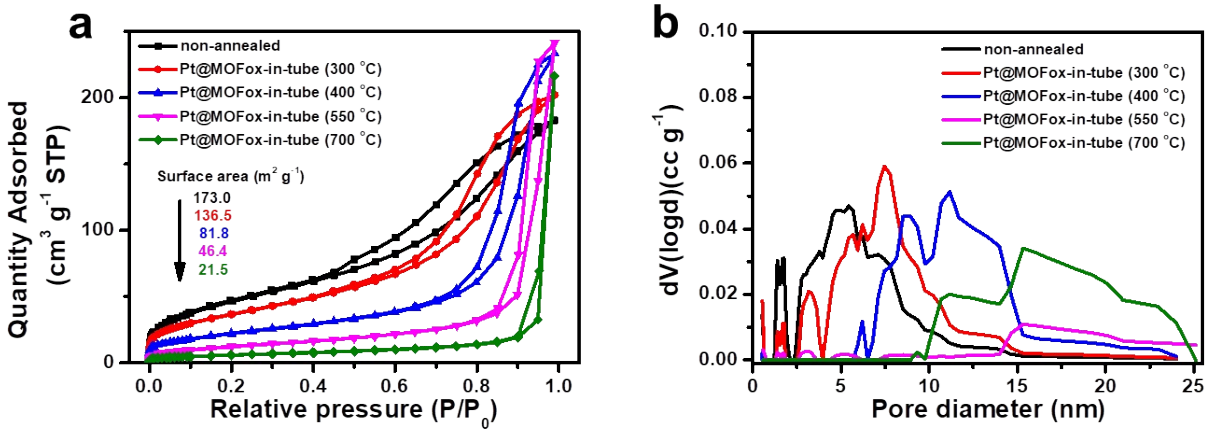

Figure S9. (a) N_2 sorption isotherms and (b) Pore size distribution of Pt@MOFox-in-tube annealed at different temperature.

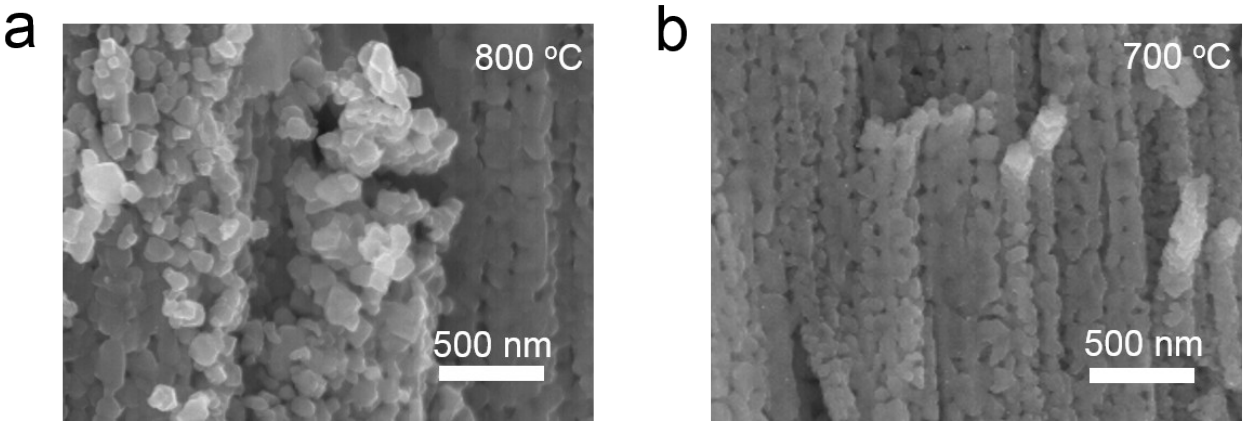

Figure S10. (a,b) Pt@MOFox-in-tube structure annealed at 800 °C and 700 °C, respectively.

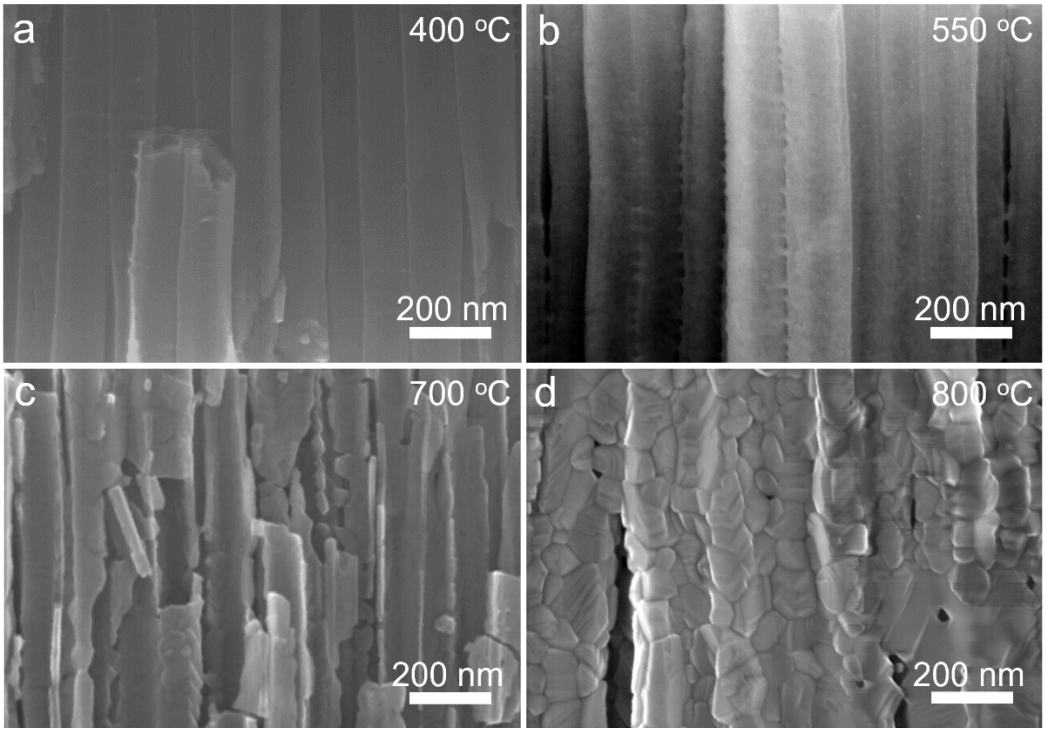

Figure S11. SEM for Pt@tube annealed at 400 °C, 550 °C, 700 °C and 800 °C, respectively.

In line with previous reports on the annealing of supported anodic TiO_2 nanotubes,[10-14] crystallization in anatase phase occurs at 250 °C - 550 °C, which gradually converts to rutile phase above 550 °C. The annealing temperature increase is also accompanied by crystal grain growth (due to coalescence of smaller grains), as evident from the additional SEM images of TiO_2 nanotubes annealed at different temperatures in Figure S11.

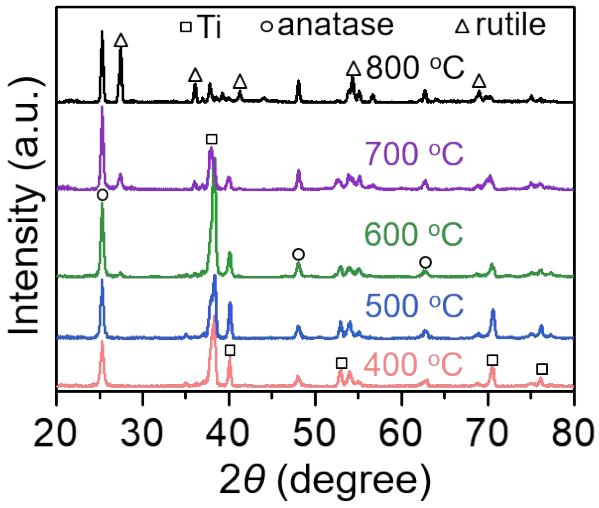

Figure S12. XRD of TiO_2 nanotubes annealed at different temperatures.[15]

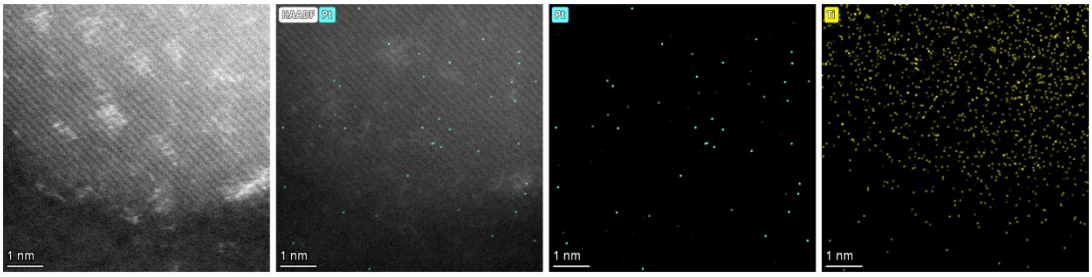

Figure S13. STEM-EDX mapping of Pt sites for Pt@MOFox-in-tube structure (annealed at 400 °C in air for 2 h, followed by immersion in a 2 mM H_2PtCl_6 solution).

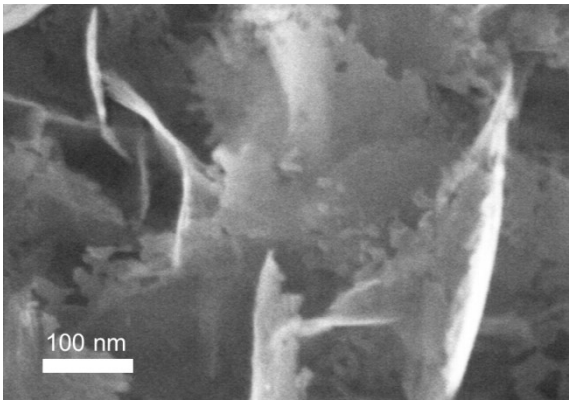

Figure S14. SEM image for Pt@MOFox-in-tube structure annealed at 400 °C.

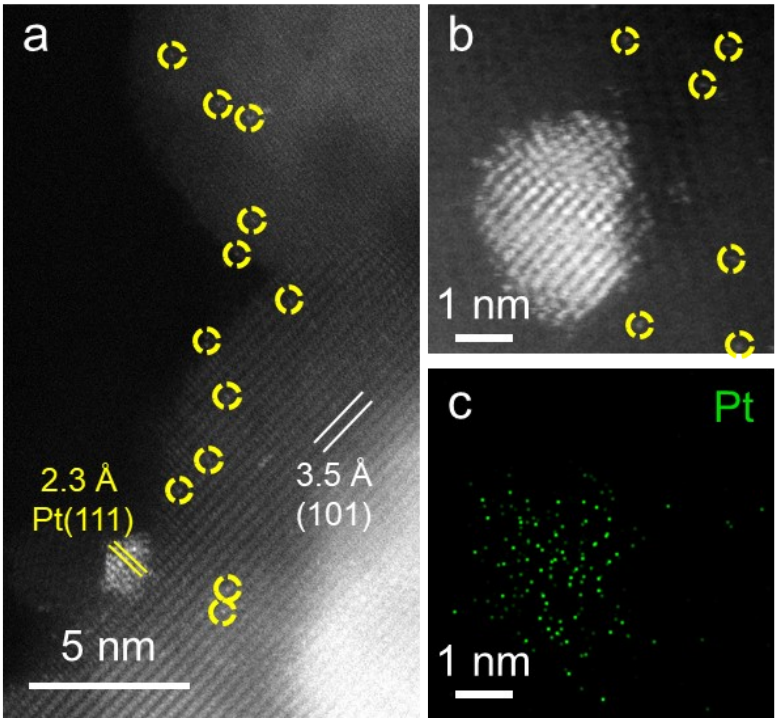

Figure S15. (a,b) HAADF-STEM images and (c) STEM-EDX mapping of Pt@MOFox-in-tube structure (annealed at 400 °C in air for 2 h and then prepared by immersion in a 2 mM H_2PtCl_6 solution) illuminated for 3 h.

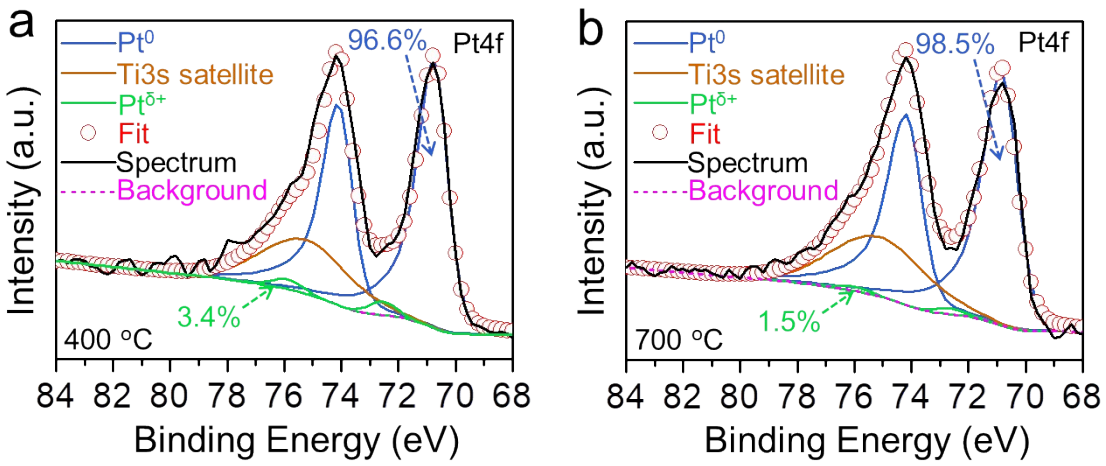

Figure S16. XPS spectra in the Pt4f region for Pt@MOFox-in-tube structures annealed at (a) 400 °C and (b) 700 °C after photocatalytic H_2 evolution for 7 days under a 365 nm LED illumination (65 mW cm^{-2}).

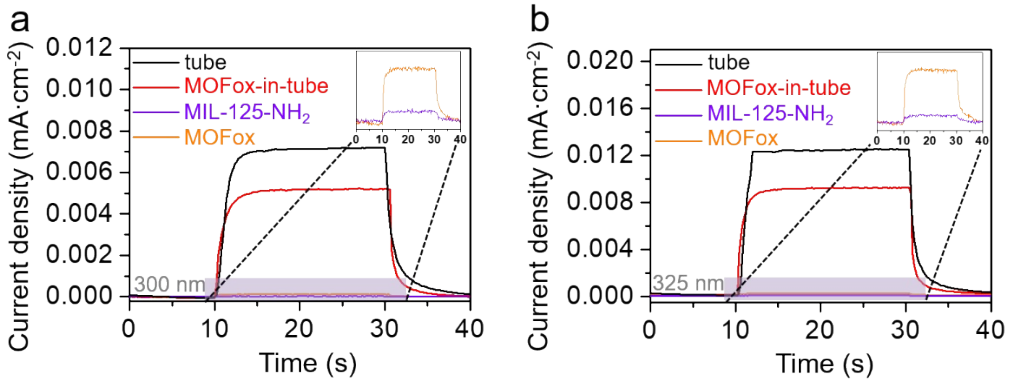

Figure S17. Transient photocurrent response for the TiO_2 nanotubes ("tube"), MOFox-in-tube structure, MOFox powder and the non-annealed MIL-125-NH_2 powder at (a) 300 nm and (b) 325 nm.

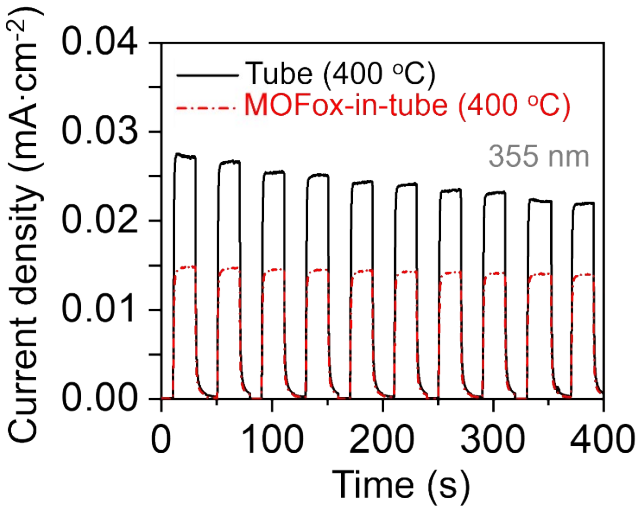

Figure S18. Cycling stability of the transient photocurrent response for Pt@MOFox-in-tube (400 °C) and TiO_2 nanotubes (400 °C).

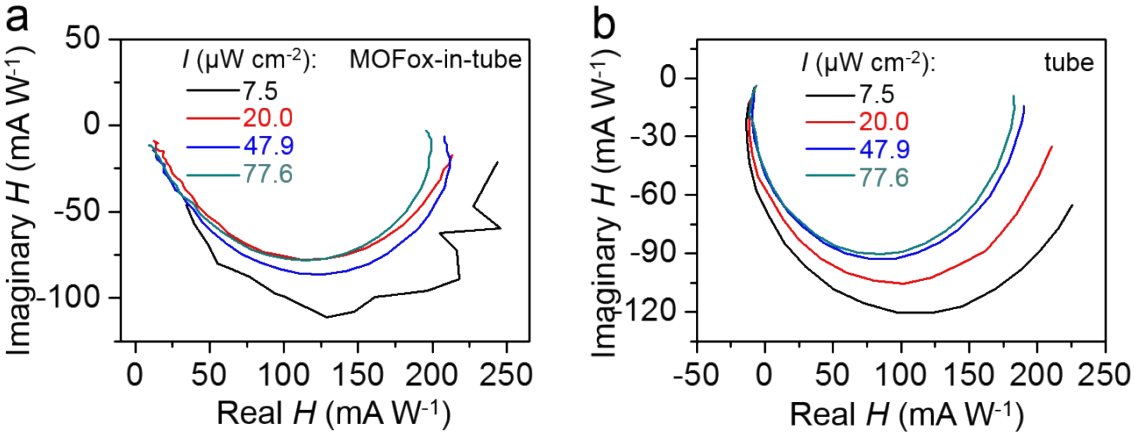

Figure S19. IMPS plots for (a) MOFox-in-tube structures and (b) TiO_2 nanotube measured under oscillating illumination (with 10% amplitude) at different intensities (I) at λ = 358 nm.

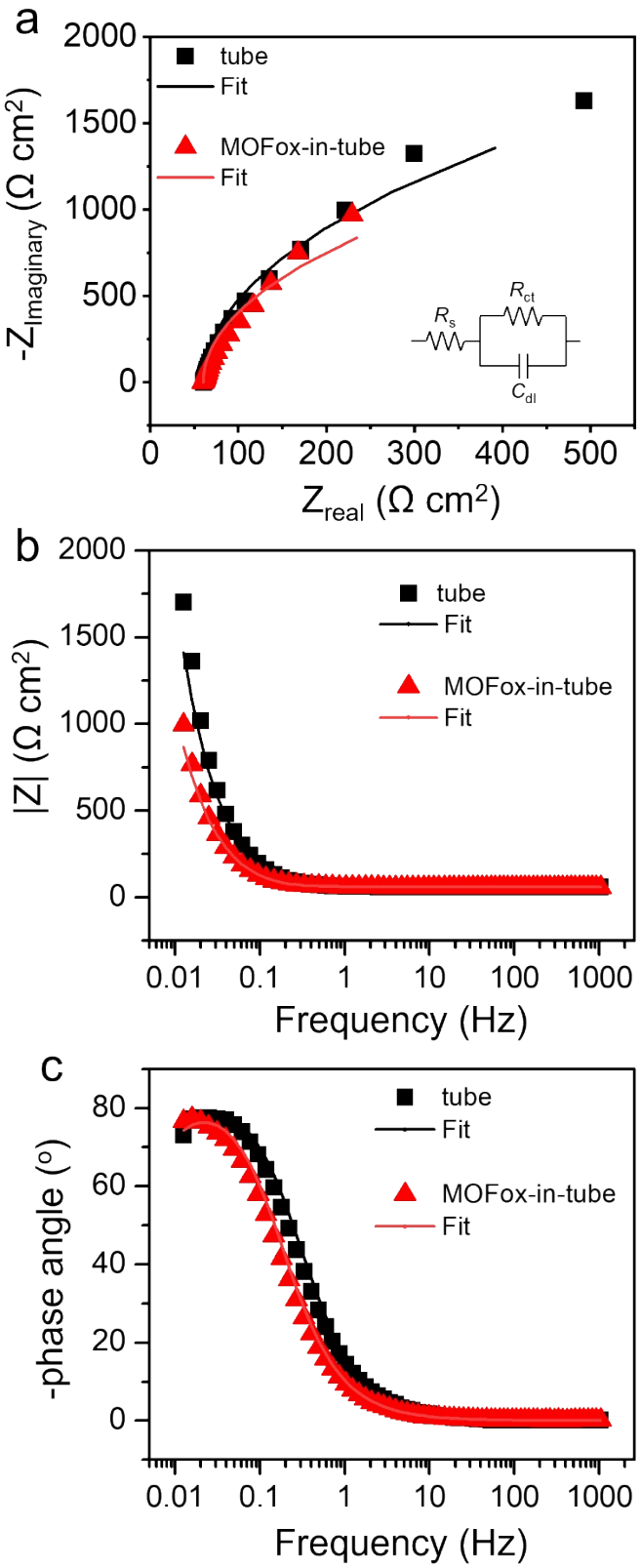

Figure S20. (a) EIS Nyquist plots and (b,c) Bode plots of MOFox-in-tube (400 °C) and TiO_2 nanotube (400 °C) recorded in the frequency range of 10^{-2} –10^{3} Hz at -0.65 V (vs. Ag/AgCl) in 0.1 M Na_2SO_4 aqueous electrolytes in dark.

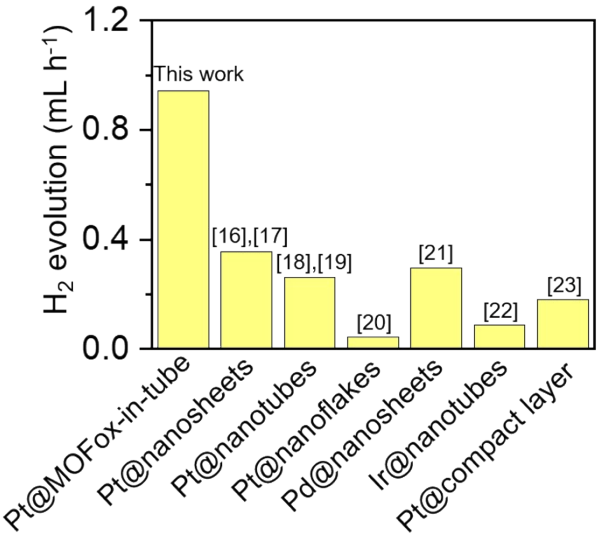

Figure S21. Comparison of the photocatalytic H_2 evolution performance of this work with the reported performance of other TiO_2 nanostructures decorated with SA co-catalysts.

In a reference experiment, TiO_2 nanotubes were firstly annealed at 400 °C for 2 h and then subjected to a hydrothermal treatment at 150 °C for 24 h. Using this experimental sequence, no MOF growth takes place inside the NTs (see Figure S22) as in-situ MOF formation relies on the partial solubility of amorphous TiO_2 nanotube walls.

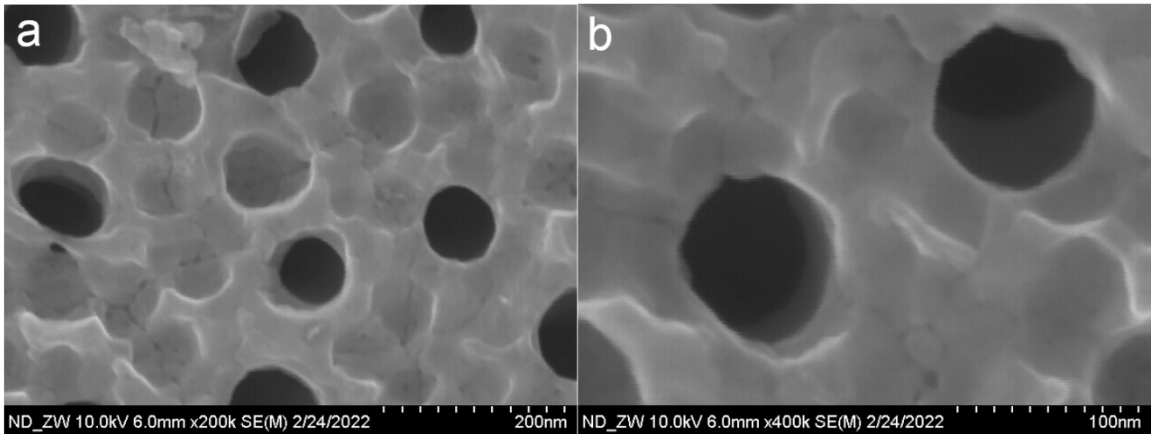

Figure S22. (a,b) SEM images of TiO_2 NTs annealed at 400 °C and subjected to the hydrothermal treatment at 150 °C for 24 h.

Table S1. Electrical parameters of the MOFox-in-tube structure and TiO_2 nanotube extracted from the EIS plots by fitting with an equivalent circuit model.

	R_s (Ω cm^2)	R_{ct} (Ω cm^2)	C_{dl} (μF cm^{-2})
Tube	60.7	5893.9	8798.4
MOFox-in-tube	60.2	4186.2	14495

References:

1. C. Zlotea, D. Phanon, M. Mazaj, D. Heurtaux, V. Guillerm, C. Serre, P. Horcajada, T. Devic, E. Magnier, F. Cuevas, G. Férey, P. L. Llewellyn, M. Latroche, *Dalton Trans.* **2011**, *40*, 4879.
2. Y. Zhang, J. Zhao, H. Wang, B. Xiao, W. Zhang, X. Zhao, T. Lv, M. Thangamuthu, J. Zhang, Y. Guo, J. Ma, L. Lin, J. Tang, R. Huang, Q. Liu, *Nat. Commun.* **2022**, *13*, 58.
3. N. Denisov, S. Qin, G. Cha, J. Yoo, P. Schmuki, *J. Electroanal. Chem.* **2020**, *872*, 114098.
4. J. Navas, R. Alcántara, C. Fernández-Lorenzo, J. Martín-Calleja, *Int. J. Energy Res.* **2012**, *36*, 193–203.
5. N. Denisov, X. Zhou, G. Cha, P. Schmuki, *Electrochim. Acta* **2021**, *377*, 137988.
6. A .S. Bondarenko, G.A . Ragoisha, A .L. Pomerantsev, in: Progress in Chemomet- rics Research, Nova Science Publishers, New York, 2005, pp. 89–102.
7. J. Guo, L. Yang, C. Zhao, Z. Gao, Y.-Y. Song and P. Schmuki, *J. Mater. Chem. A*, 2021, **9**, 14911-14919.
8. J. Guo, L. Yang, C. Zhao, Z. Gao, Y.-Y. Song and P. Schmuki, *J. Mater. Chem. A*, 2021, **9**, 14911-14919.
9. T.C. Narayan, T. Miyakai, S. Seki, M. Dincă, *J. Am. Chem. Soc.*, **2012**, *134*, 12932–12935.
10. S. P. Albu, H. Tsuchiya, S. Fujimoto and P. Schmuki, *European Journal of Inorganic Chemistry*, 2010, **2010**, 4351-4356.
11. A. Tighineanu, T. Ruff, S. Albu, R. Hahn and P. Schmuki, *Chemical Physics Letters*, 2010, **494**, 260-263.
12. A. Tighineanu, S. P. Albu and P. Schmuki, *physica status solidi (RRL) – Rapid Research Letters*, 2014, **8**, 158-162.
13. S. Bauer, A. Pittrof, H. Tsuchiya and P. Schmuki, *Electrochemistry Communications*, 2011, **13**, 538-541.
14. D. Fang, Z. Luo, K. Huang and D. C. Lagoudas, *Applied Surface Science*, 2011, **257**, 6451-6461.
15. X. Chen, S. Qin, N. Denisov, S.-Z. Kure-Chu and P. Schmuki, *Electrochim. Acta*, 2023, **446**, 142081.
16. N. Denisov, S. Qin, J. Will, B. N. Vasiljevic, N. V. Skorodumova, I. A. Pašti, B. B. Sarma, B. Osuagwu, T. Yokosawa, J. Voss, J. Wirth, E. Spiecker and P. Schmuki, *Adv. Mater.*, 2023, **35**, 2206569.
17. S. Qin, N. Denisov, J. Will, J. Kolařík, E. Spiecker and P. Schmuki, *Solar RRL*, 2022, **6**, 2101026.
18. Z. Wu, I. Hwang, G. Cha, S. Qin, O. Tomanec, Z. Badura, S. Kment, R. Zboril and P. Schmuki, *Small*, 2021, 2104892.
19. I. Hwang, A. Mazare, J. Will, T. Yokosawa, E. Spiecker and P. Schmuki, *Adv. Funct. Mater.*, 2022, **n/a**, 2207849.
20. G. Cha, A. Mazare, I. Hwang, N. Denisov, J. Will, T. Yokosawa, Z. Badura, G. Zoppellaro, A. B. Tesler, E. Spiecker and P. Schmuki, *Electrochim. Acta*, 2022, **412**, 140129.
21. G. Cha, I. Hwang, S. Hejazi, A. S. Dobrota, I. A. Pašti, B. Osuagwu, H. Kim, J. Will, T. Yokosawa, Z. Badura, Š. Kment, S. Mohajernia, A. Mazare, N. V. Skorodumova, E. Spiecker and P. Schmuki, *iScience*, 2021, **24**, 102938.
22. X. Zhou, I. Hwang, O. Tomanec, D. Fehn, A. Mazare, R. Zboril, K. Meyer and P. Schmuki, *Adv. Funct. Mater.*, 2021, **31**, 2102843.
23. S. Qin, J. Will, H. Kim, N. Denisov, S. Carl, E. Spiecker and P. Schmuki, *ACS Energy Lett.*, 2023, **8**, 1209-1214.